Supporting Information

Flexibility of the petunia strigolactone receptor DAD2 promotes interaction with signaling partners

Hui Wen Lee[1,2†#], Prachi Sharma[1,2†‡], Bart J. Janssen[1], Revel S. M. Drummond[1], Zhiwei Luo[1], Cyril Hamiaux[1], Thomas Collier[3], Jane Allison[2,4,5], Richard D. Newcomb[1,2] and Kimberley C. Snowden[1*]

The following supporting information is included:

Table S1. Data collection and refinement statistics for the $DAD2^{N242I}$ and $DAD2^{D166A}$ crystals.

Figure S1. DAD2 receptor showing the location of residues, F135, D166, S96 and N242I.

Figure S2. Preliminary yeast two-hybrid analysis of some additional DAD2 mutants.

Figure S3. Western blots for the yeast 2-hybrid experiments.

Figure S4. DSF assays of DAD2 and DAD2 mutants.

Figure S5. Structural comparison of $DAD2^{WT}$ and molecule B of $DAD2^{N242I}$.

Figure S6. MES bound within the catalytic cavity of the $DAD2^{N242I}$ protein.

Figure S7: Thermal stability of $DAD2^{WT}$ and $DAD2^{N242I}$ in the presence of varying concentration of MES.

Figure S8. Per-residue root-mean-square-fluctuation (RMSF) of $DAD2^{WT}$ and $DAD2^{N242I}$ MD simulations.

Figure S9. Structural comparison of $DAD2^{WT}$ with molecule B of $DAD2^{D166A}$.

Figure S10. Position of the D167 residue in the open and closed AtD14 receptor.

Figure S11. Model of the consequences of selected mutations of DAD2 on protein-protein interactions.

Figure S12. Enzyme activity of wild-type $DAD2^{WT}$ and $DAD2^{C89Q}$ (C89Q).

Movie S1 is included in a separate file. $DAD2^{WT}$ and $DAD2^{N242I}$ MD simulation movements.

Table S1. Data collection and refinement statistics for the DAD2^{N242I} and DAD2^{D166A} crystals. Values in parenthesis belong to the last resolution shell

	DAD2^{N242I}	**DAD2^{D166A}**
PDB entry code	6UH8	6UH9
Space group	$P6_5$	P1
Cell parameters		
a (Å)	133.74	36.69
b (Å)	133.74	56.53
c (Å)	99.76	68.04
α (°)	90	94.47
β (°)	90	94.67
γ (°)	120	108.83
Data collection		
Wavelength (Å)	0.953736	0.9537
Number of images	3600	360
Oscillation angle (°)	0.1	1
Total reflections	2648154	291626
Unique reflections	138411	75017
Resolution range (Å)	45.81 -1.58 (1.61 - 1.58)	30.21-1.52 (1.55 - 1.52)
R_{merge}	0.088 (2.188)	0.089 (0.669)
$CC_{1/2}$	1.000 (0.728)	0.997 (0.721)
I / σ (I)	20.3 (1.6)	7.8 (1.6)
Completeness (%)	100 (100)	91.6 (91.6)
Multiplicity	19.1 (18.9)	3.9 (3.9)
B_{wilson} (Å^2)	17.6	9.8
Refinement		
Resolution (Å)	1.58	1.52
Reflections	137623	74863
Total number of atoms	4792	4938
TLS group	2 (one per monomer)	2 (one per monomer)
R_{work}/ R_{free}	13.8/16.5 (24.6/ 26.7)	17.1/ 19.9 (26.1/ 27.3)
R.M.S.D bond (Å)	0.0132	0.0092
R.M.S.D angle (°)	1.7403	1.5128
Average B factors (Å^2; all atoms)	29.4	19.9
Ramachandran statistics (%)		
Residues in favour region	98.0	98.5
Residues in allowed region	2.5	1.5
Residues in outlier region	2.0	0

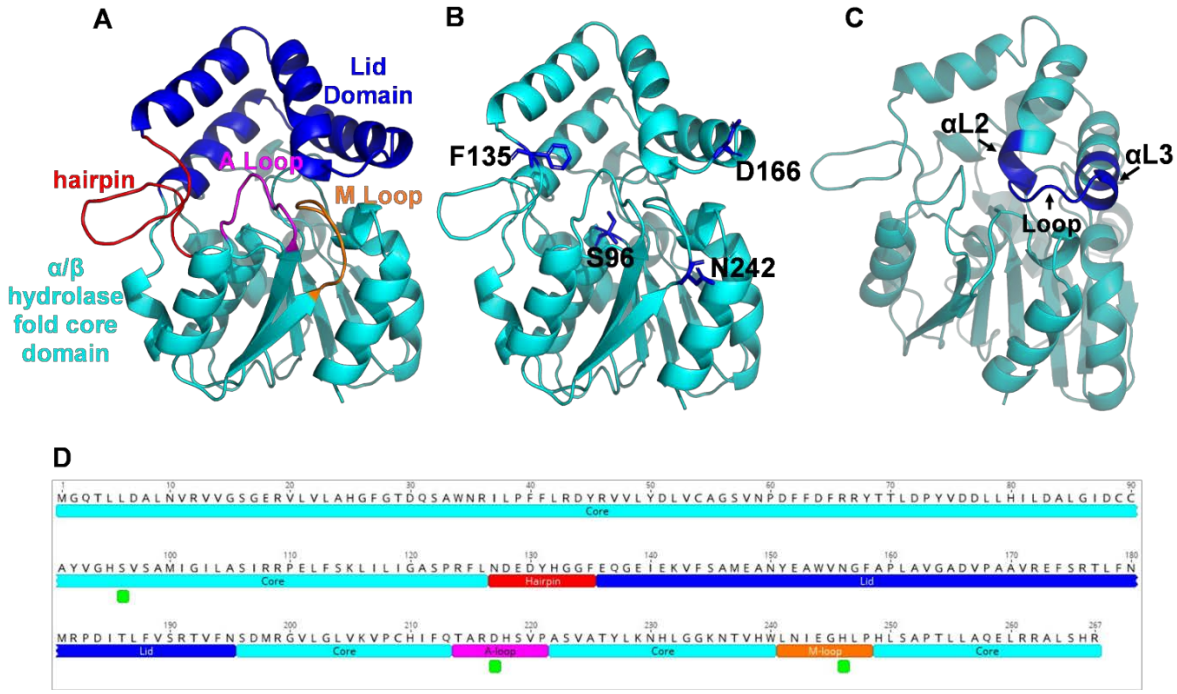

Figure S1. DAD2 receptor showing the location of residues, F135, D166, S96 and N242I. **A)** DAD2 receptor showing the lid domain (blue), hairpin (red), α/β hydrolase fold core domain (cyan), A loop (magenta) and M loop (orange). **B)** DAD2 receptor (cyan) showing the location of residues, F135, D166, S96 and N242 (shown in stick representation in blue). **C)** The αL2-loop-αL3 region of the lid domain (blue) of DAD2^{N242I} (cyan). **D)** Sequence view of DAD2 with residue numbering, showing the location and the same coloring scheme of the protein regions shown in **A**, as well as active site residues marked in green.

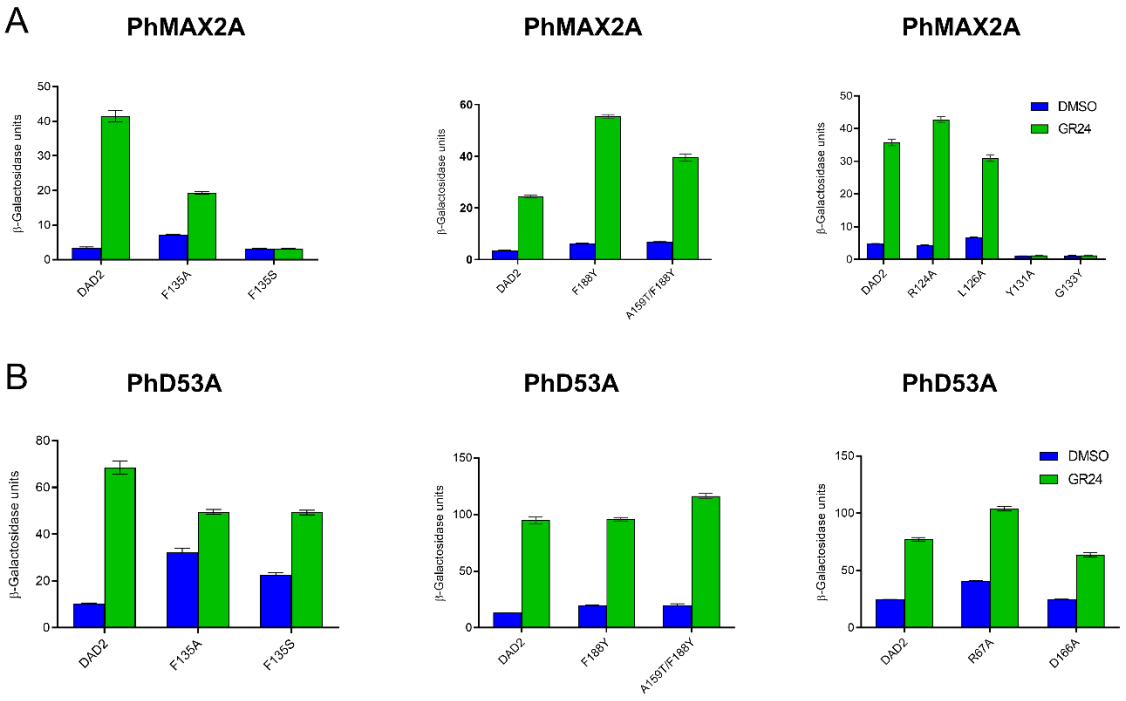

Figure S2. Preliminary yeast two-hybrid analysis of some additional DAD2 mutants. Graphs shown in **A** show interactions between DAD2 or DAD2 mutants with PhMAX2A; graphs in **B** show interactions between DAD2 or DAD2 mutants with PhD53A. Interactions shown in each graph were quantified in the presence and absence of GR24 (5 μM for interactions with PhMAX2A and 1 μM for interactions with PhD53A) using yeast two-hybrid β-galactosidase liquid culture assays. Locations of mutant residues can be determined from Figure S1D. Data shown are means ± S.E.M., n = 3.

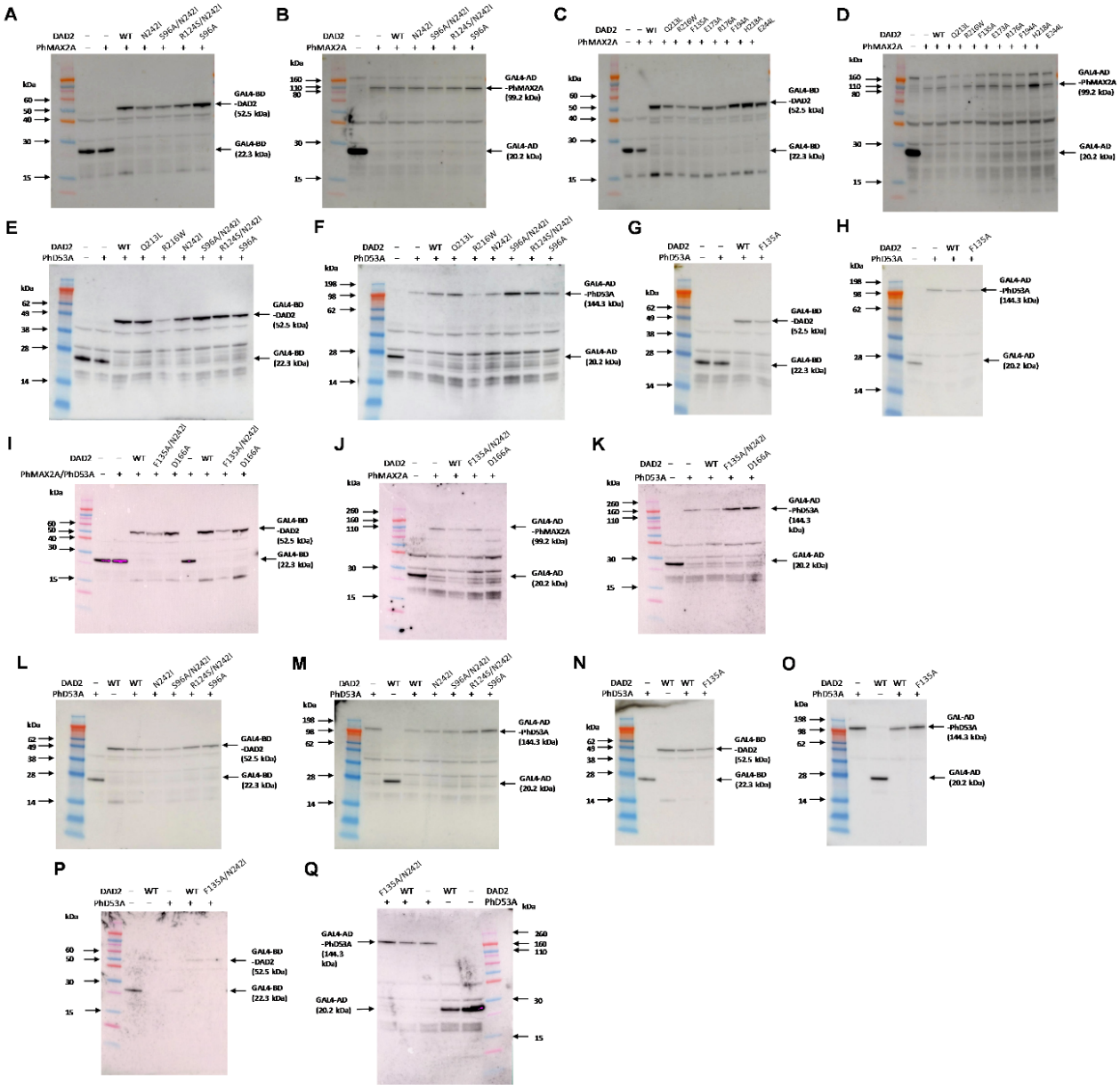

Figure S3. Western blot analyses for the yeast two-hybrid experiments. Western blot analyses showed the presence of the binding domain either alone (denoted by (–)) or as a fusion protein with DAD2 **(A, C, E, G, I, L, N, P)**, as well as the presence of the activation domain either alone (denoted by (–)) or as a fusion protein with PhMAX2A **(B, D, J)** or PhD53A **(F, H, K, M, O, Q).** PhMAX2A/PhD53A and wild-type DAD2 are indicated by (+) and WT, respectively. The presence of the yeast two-hybrid fusion proteins in the diploid interaction test strains was confirmed by detection of the Gal4 DNA binding (Gal4-BD) and Gal4 transcription activation (Gal4-AD) domains by monoclonal antibody (GAL4-DBD and GAL4-TA, respectively; Santa Cruz Biotechnology). Note that yeast strains were included in these western blot analyses for additional mutants that are not shown in Figures 1-2. Loading control was assessed by the non-specific binding of the secondary antibody (Biorad 170-6516) to a 40 kDa protein present in all the yeast strains. Size standards shown are either the Novex® Sharp or the SeeBlue® Plus2 pre-stained protein standards (Life Technologies). The presence of the expected fusion proteins in the yeast strains that were used to generate the data in Figure 1A-C (DAD2-PhMAX2A) is shown in panels A-D, I and J, where A, C and I show the detection of the Gal4-BD fusion proteins and B, D, and J show the detection of the corresponding Gal4-AD fusion proteins. Testing of the yeast strains shown

in Figure 1D-F (DAD2-PhD53A) is shown in panels E-I, and K, where E, G and I show the detection of the Gal4-BD fusion proteins and F, H, and K show the detection of the corresponding Gal4-AD fusion proteins. Testing of the yeast strains shown in Figure 2A (DAD2 mutants S96A and N242I) is shown in panels L and M where L shows the detection of the Gal4-BD fusion proteins and M shows the detection of the corresponding Gal4-AD fusion proteins. Testing of the yeast strains shown in Figure 2B (DAD2 mutants F135A and N242I) is shown in panels L-Q, where L, N and P show the detection of the Gal4-BD fusion proteins and M, O, and Q show the detection of the corresponding Gal4-AD fusion proteins.

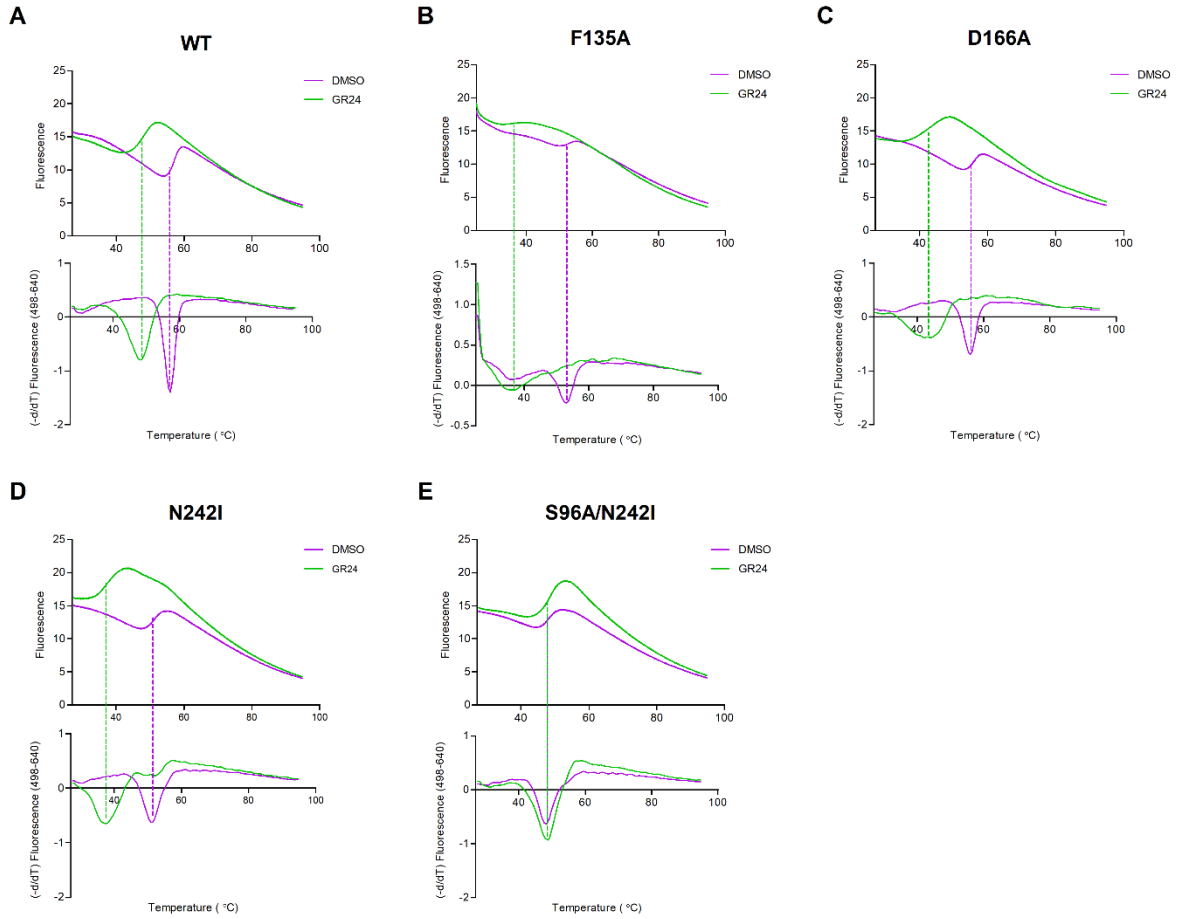

Figure S4. DSF assays of DAD2 and DAD2 mutants. Experimental melting curves (top) and derivatives of the melting curves (bottom) for **(A)** DAD2 (WT), **(B)** DAD2^{F135A}, **(C)** DAD2^{D166A}, **(D)** DAD2^{N242I}, and **(E)** DAD2$^{S96A/N242I}$ in the presence and absence of 250 µM GR24. The melting temperatures (T_m) of the proteins (see Table 2) are indicated by dotted vertical lines. All experiments were conducted in triplicate.

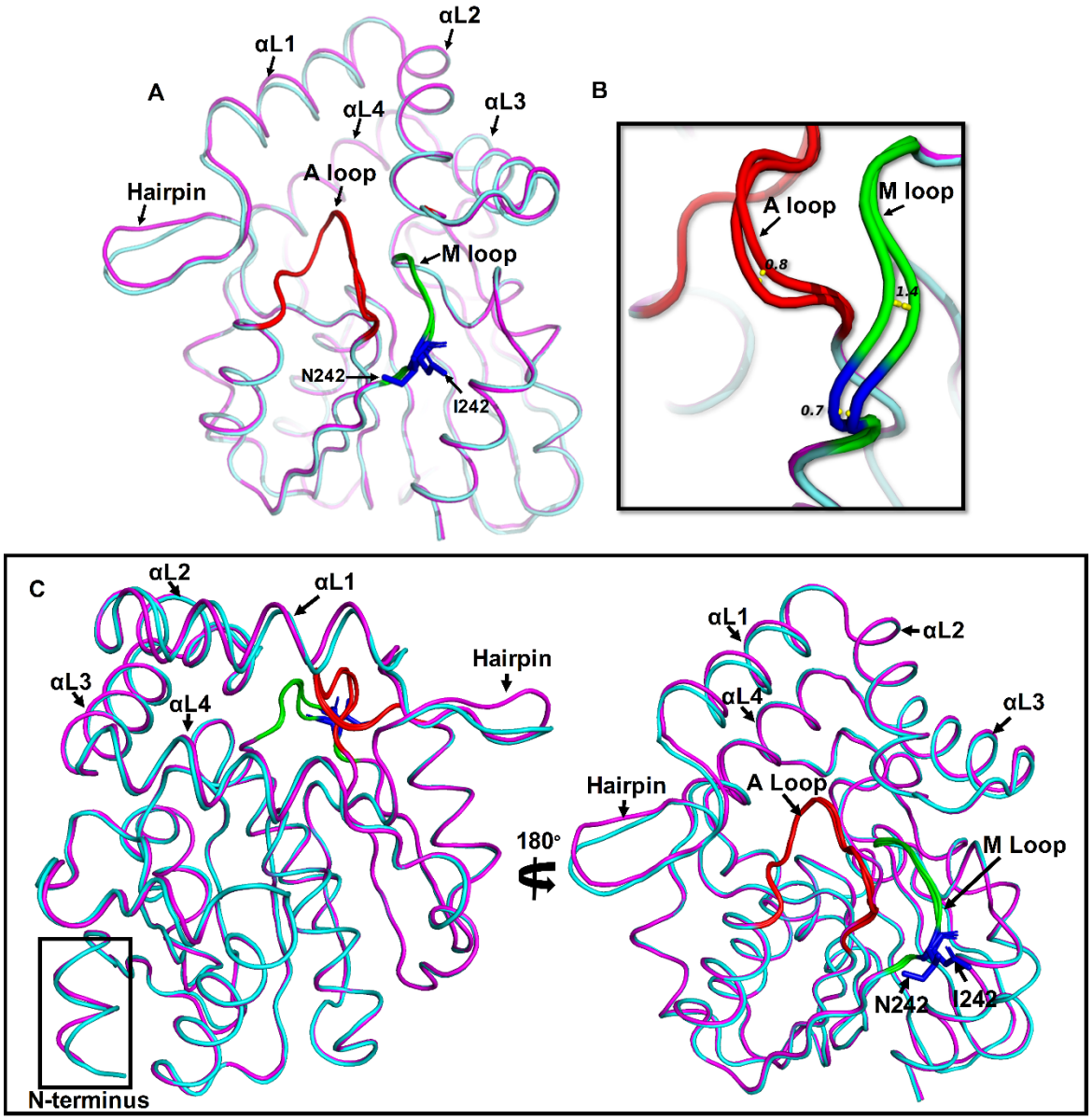

Figure S5. Structural comparison of DAD2^{WT} and molecule B of DAD2^{N242I}. **(A)** Structure of molecule B of DAD2^{N242I} protein (cyan) aligned to the structure of DAD2^{WT} (magenta, PDB ID: 4DNP; (Hamiaux et al., 2012)). The N242 and I242 residues are shown in stick representation in blue, the A loop in red and the M loop in green. **(B)** The displacement of the A and M loops (in Å, shown as yellow dotted lines) in molecule B of DAD2^{N242I} in comparison with DAD2^{WT}. **(C)** Side and front profile of the aligned DAD2^{N242I} and DAD2^{WT} structures showing the N-terminus, lid helices (αL1, αL2, αL3 and αL4), hairpin, A loop and the M loop. The DAD2^{N242I} protein also included a C89Q mutation to facilitate crystallization.

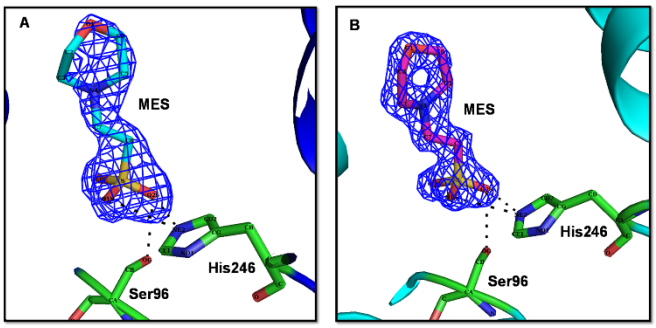

Figure S6. MES bound within the catalytic cavity of the DAD2^{N242I} protein. MES (shown in stick representation) bound within the catalytic cavity of molecule A (**A**) and molecule B (**B**) of the DAD2^{N242I} protein. Hydrogen bonds are shown by dotted black lines, His246 and Ser96 are shown in stick representation and coloured by atoms (oxygen is shown in red, nitrogen in blue and carbon in green). The blue mesh around the MES molecule is the 2Fo-Fc electron density map contoured at 1.5 σ.

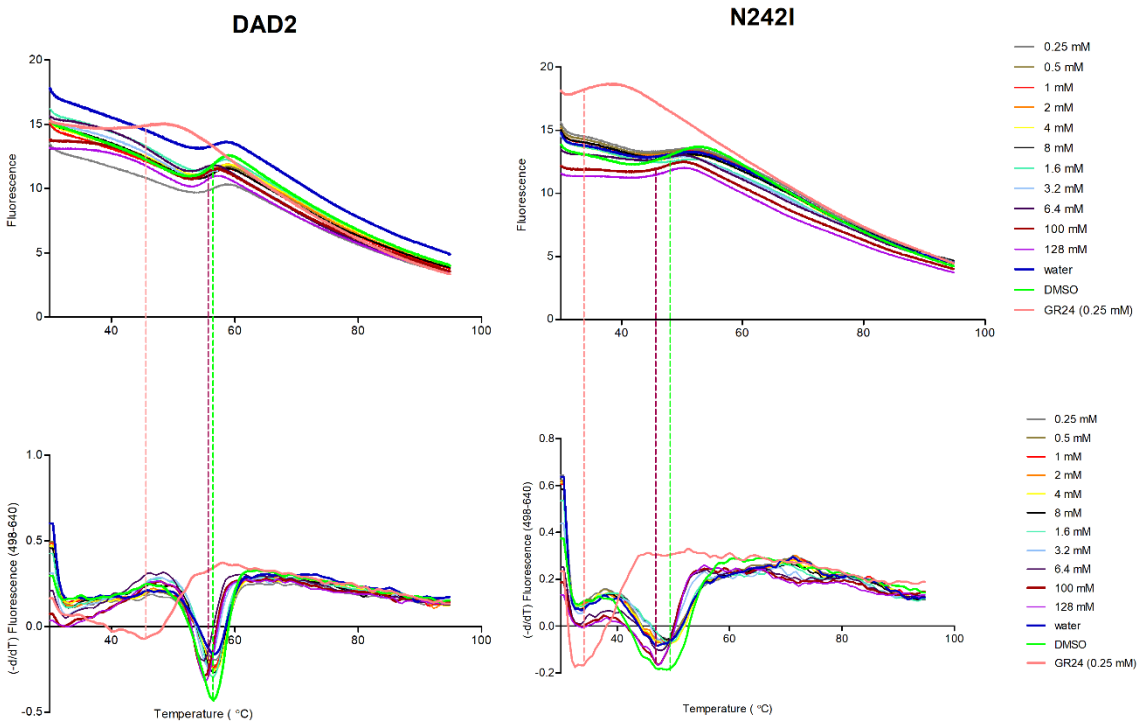

Figure S7: Thermal stability of DAD2^{WT} and DAD2^{N242I} in the presence of varying concentrations of MES. The DSF assay results for DAD2^{WT} (DAD2; left) and DAD2^{N242I} (N242I; right). The top graphs are the melting curves, with the bottom graphs showing the derivatives of the melting curves. The thermal stability was tested using DSF assays that were performed using 10 µM of DAD2^{WT}/DAD2^{N242I} protein in the presence of varying concentration of MES. 0.25 mM MES is shown in grey, 0.5 mM in olive green, 1 mM in red , 4 mM shown in yellow, 8 mM in black, 16 mM in cyan, 32 mM in light blue, 64 mM in violet, 100 mM in maroon, 128 mM in purple, GR24 in pink, DMSO in green, water in blue. The dotted lines depict the melting temperature (T_m) exhibited by the two proteins in the presence of *(rac)*-GR24 (pink), DMSO (green) and 1 mM MES as used in crystallisation experiments (maroon).

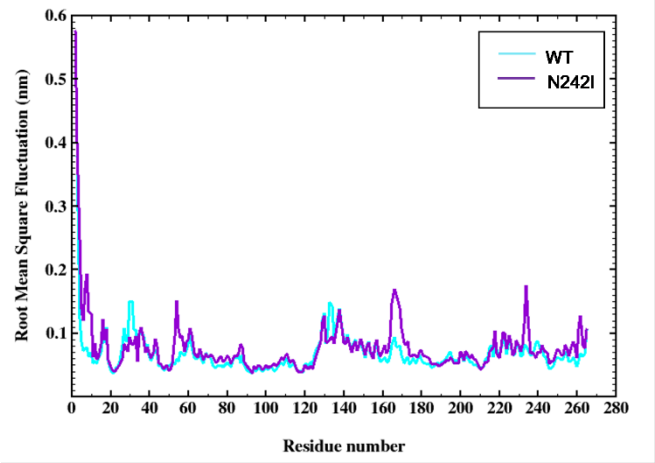

Figure S8. Per-residue root-mean-square-fluctuation (RMSF) of $DAD2^{WT}$ and $DAD2^{N242I}$ MD simulations. RMSF of each residue from its average position depicting the average fluctuation in the atomic positions of each residue of $DAD2^{WT}$ (WT; cyan) and $DAD2^{N242I}$ (N242I; violet) during the MD simulation.

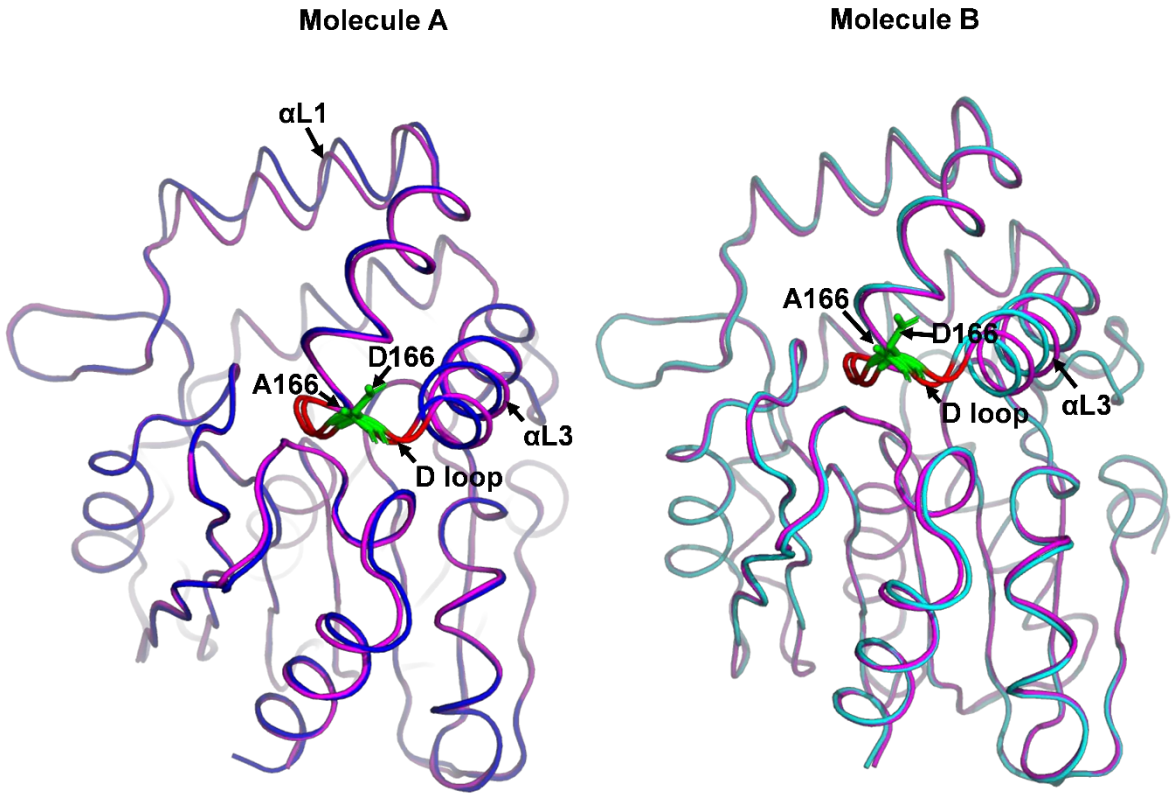

Figure S9. Structural comparison of DAD2^{WT} with DAD2^{D166A}. The structure of DAD2^{WT} (magenta; PDB ID: 4DNP; (Hamiaux et al., 2012)) aligned onto the structure of molecule A of DAD2^{D166A} (left and shown in blue) and molecule B of DAD2^{D166A} (right and shown in cyan). The loop containing the D166/A166 residue (also referred to here as the D loop) is shown in red, the D166 residue of DAD2^{WT} and A166 residue of DAD2^{D166A} are shown in stick representation in green. The DAD2^{D166A} protein also included a C89Q mutation to facilitate crystallization.

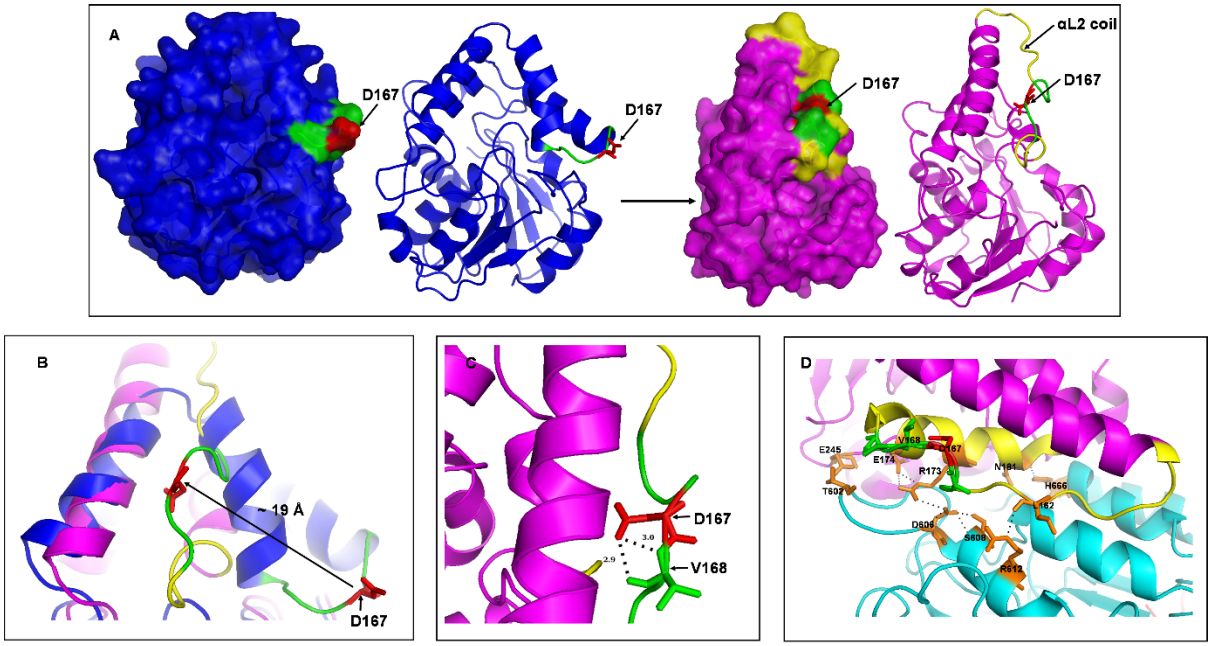

Figure S10. Position of the D167 residue in the open and closed AtD14 receptor. **(A)** Shows the open (blue) and closed conformation (magenta) of the AtD14 receptor. In the two conformations, the D167 residue (shown in red) goes from being exposed, in the open conformation, to being completely buried in the closed conformation. The D loop is shown in green. The newly formed αL2 coil in the closed conformation is shown in yellow. The open conformation is depicted by the apo-AtD14 structure sourced from PDB (PDB ID: 4IH4 (Zhao et al., 2013)) and the closed conformation is represented by the AtD14 structure from the AtD14-D3-ASK1 complex, sourced from PDB (PDB ID: 5HZG; (Yao et al., 2016)). **(B)** Shows the displacement of the D167 residue, which moves by approximately 19 Å from the open (blue) to the closed (magenta) conformation of the receptor. **(C)** Shows the D167 residue forming two H-bonds (shown as black dashed lines) with the backbone atom of the adjacent valine residue, V168. **(D)** A close-up view showing the residues involved in AtD14-D3 interaction. The AtD14 and D3 proteins are shown in magenta and cyan, respectively. The interacting residues between AtD14 and D3 are shown in stick representations in orange, whereas the major interaction surface on AtD14 for D3 binding is shown in yellow. The D167 residue (red) and other residues of the D loop (green) are not directly involved in AtD14-D3 interaction but form part of the interaction surface. The figure was created using the crystal structure of AtD14-D3-ASK1 complex, sourced from PDB (PDB ID: 5HZG; (Yao et al., 2016)).

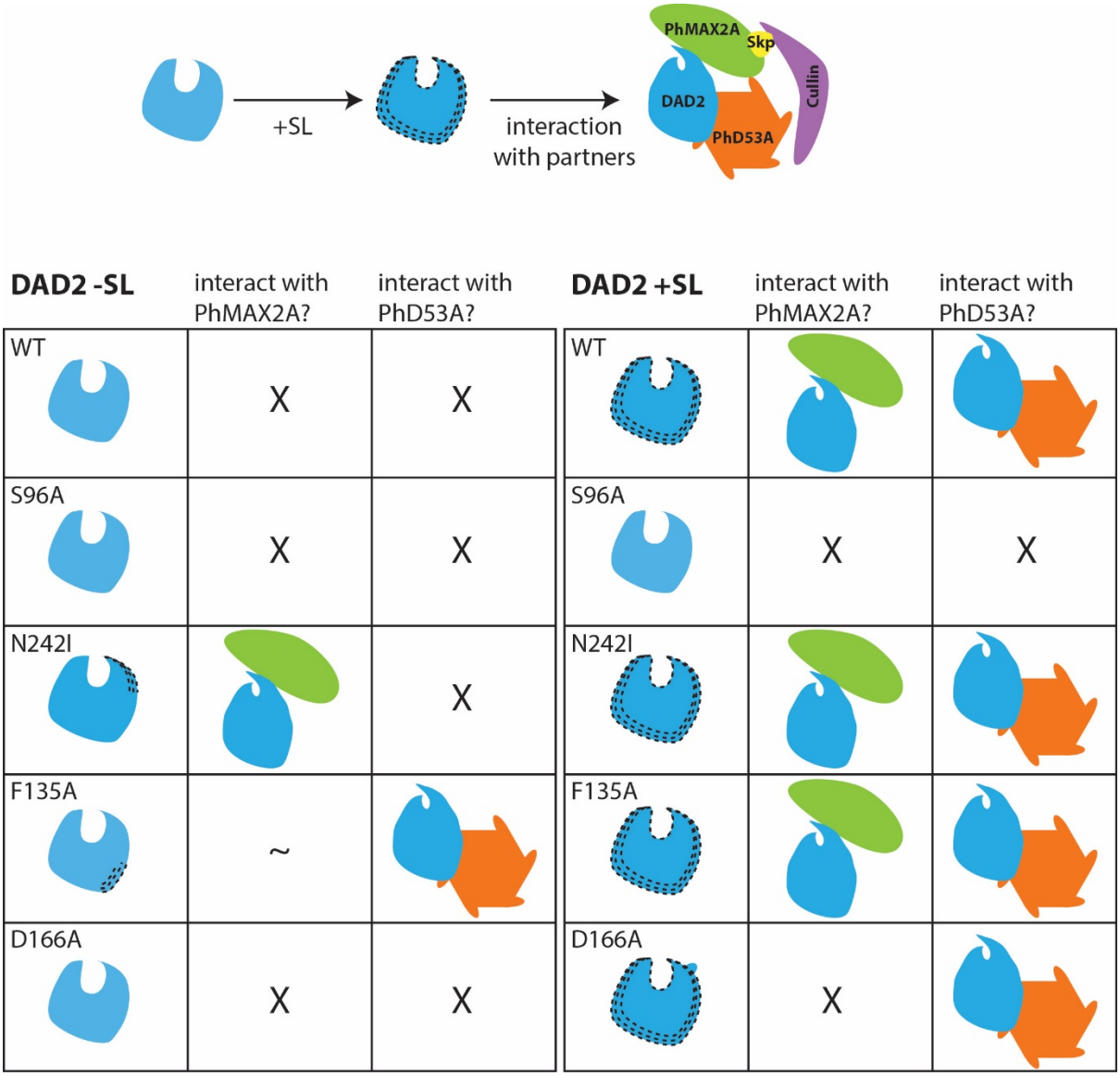

Figure S11. Model of the consequences of selected mutations of DAD2 on protein-protein interactions. DAD2 protein may gain flexibility in the presence of SL, allowing interaction with the F-box protein PhMAX2A and the target protein PhD53A. The interaction of binding partners stimulates a conformational change in DAD2. The top panel shows a summary of these changes to DAD2 and the interactions. In the bottom panels, the consequences of selected mutations of the DAD2 protein are represented by dotted lines showing changes to the flexibility of DAD2 or a change in shape, in the absence or presence of SL. Note that there may be more than one type of conformational change to DAD2 possible depending on the partners that are bound (PhMAX2A, PhD53A or both), for simplicity these are all given the same representation. The N242I and F135A mutant proteins likely have some regions with increased flexibility compared to the WT protein in the absence of SL. The D166A mutant is predicted to have similar flexibility compared to WT, however the mutation present in this protein is unable to achieve or maintain the conformational change required for interaction with PhMAX2A.

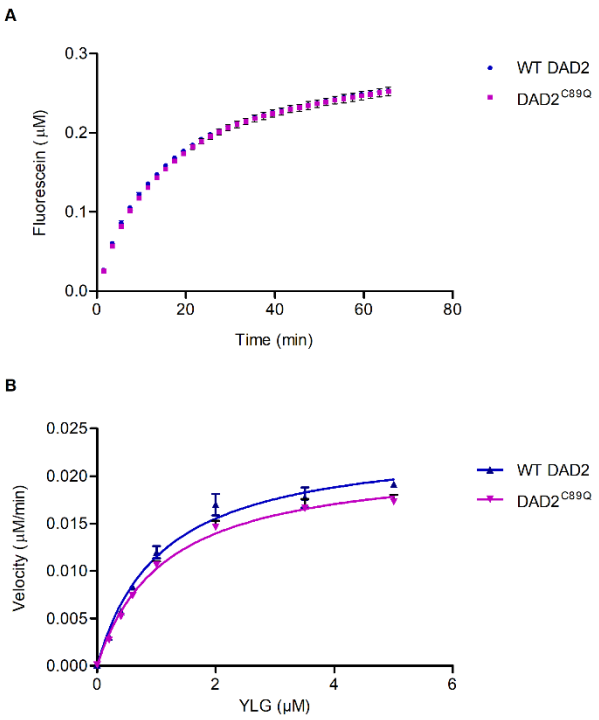

Figure S12. Enzyme activity of wild-type DAD2^{WT} and DAD2^{C89Q} (C89Q). **(A)** Time course hydrolysis of 1 µM YLG by DAD2^{WT} (WT DAD2) and DAD2^{C89Q} (C89Q) (0.34 µM) over 60 min. Each data point is the mean ± S.E.M. of three technical replicates. **(B)** Hydrolysis of YLG by WT DAD2 and DAD2^{C89Q} (C89Q) (0.34 µM) at various YLG concentrations. Each data point is the average of three technical replicates.